

Deep Quantum Error Correction

Yoni Choukroun¹ Lior Wolf¹

Abstract

Quantum error correction codes (QECC) are a key component for realizing the potential of quantum computing. QECC, as its classical counterpart (ECC), enables the reduction of error rates, by distributing quantum logical information across redundant physical qubits, such that errors can be detected and corrected. In this work, we efficiently train novel deep quantum error decoders. We resolve the quantum measurement collapse by augmenting syndrome decoding to predict an initial estimate of the system noise, which is then refined iteratively through a deep neural network. The logical error rates calculated over finite fields are directly optimized via a differentiable objective, enabling efficient decoding under the constraints imposed by the code. Finally, our architecture is extended to support faulty syndrome measurement, to allow efficient decoding over repeated syndrome sampling. The proposed method demonstrates the power of neural decoders for QECC by achieving state-of-the-art accuracy, outperforming, for a broad range of topological codes, the existing neural and classical decoders, which are often computationally prohibitive.

1. Introduction

Error Correcting Codes (ECC) are required in order to overcome computation and transmission corruption in almost every computation device (Shannon, 1948; Lidar & Brun, 2013). The demands of high-performance hardware and communication networks have led to the rapid development of classical ECC theory and algorithms (MacKay et al., 2003). Quantum systems are known for being extremely

¹The Blavatnik School of Computer Science, Tel Aviv University. Correspondence to: Yoni Choukroun <choukroun.yoni@gmail.com>, Lior Wolf <wolf@cs.tau.ac.il>.

noisy (Ballance et al., 2016; Huang et al., 2019; Foxen et al., 2020). However, adapting existing classical ECC methods to the quantum domain (QECC) is not straightforward (Raimond & Haroche, 1996).

The first difficulty in applying ECC-based knowledge to QECC arises from the no-cloning theorem for quantum states (Wootters & Zurek, 1982), which asserts that it is impossible to clone a quantum state and thus add arbitrarily redundant parity information, as done in classical ECC. The second challenge is the need to detect and correct quantum continuous bit-flips, as well as phase-flips (Cory et al., 1998; Schindler et al., 2011), while classical ECC addresses only bit-flip errors. A third major challenge is the wave function collapse phenomenon: any direct measurements (while being standard in ECC) of the qubits would cause the wave function to collapse and erase the encoded quantum information (Neumann et al., 1955).

Shor (1995) proposed the first quantum error correction scheme, demonstrating that these challenges can be overcome. Subsequently, threshold¹ theorems have shown that increasing the distance of a code will result in a corresponding reduction in the logical error rate, signifying that quantum error correction codes can arbitrarily suppress the logical error rate (Aharonov & Ben-Or, 1997; Kitaev, 1997a; Preskill, 1998). This distance increase is obtained by developing encoding schemes that reliably store and process information in a logical set of qubits, by encoding it redundantly on top of a larger set of less reliable physical qubits (Nielsen & Chuang, 2002).

Most current QECC methods fall in the category of stabilizer codes, which can be seen as a generalization of the classical linear codes (Gottesman, 1997). Similarly to the classical parity check constraints, a group of stabilizer operators can provide a syndrome, while preserving the logical quantum states and enabling error detection.

Optimal decoding is defined by the unfeasible NP-hard maximum likelihood rule (Dennis et al., 2002; Kuo & Lu, 2020). Despite considerable research dedicated to the design of codes with some additional algebraic structure, which can support efficient decoding, such QECC decoders remain in-

¹In this context, a threshold is the minimal error rate such that adding more physical qubits in the code results in fewer logical errors.

efficient or impractical (Calderbank & Shor, 1996; Schindler et al., 2011). One of the most promising categories of codes is that of topological codes, particularly surface codes, which originated from Toric codes (Bravyi & Kitaev, 1998; Freedman & Meyer, 2001; Kitaev, 1997a;c; Dennis et al., 2002; Kitaev, 2003). Given boundary conditions, the idea is to encode every logical qubit in a 2D lattice of physical qubits. This local design of the code via nearest-neighbors coupled qubits allows the correction of a wide range of errors. Under certain assumptions, surface codes provide an exponential reduction in the error rate (Kitaev, 1997a;b).

In this work, we present a novel neural quantum decoding algorithm that can be applied to any stabilizer code. We first predict an approximation of the system noise, turning the quantum syndrome decoding task into a form that is compliant with the classical ECC Transformer decoder (Choukroun & Wolf, 2022), which is based on the parity-check matrix. This initial estimate of the noise is reminiscent of Monte Carlo Markov Chains methods (Wootton & Loss, 2012), which start the decoding process with a random error that is compatible with the syndrome, and then refine it iteratively. Second, in order to support logical error optimization, we develop a novel differentiable way of learning under the Boolean algebra constraints of the logical error rate metric. Finally, we propose a new architecture that is capable of performing quantum error correction under faulty syndrome measurements. As far as we can ascertain, this is the first time that (i) a Transformer architecture (Vaswani et al., 2017) is applied to the quantum syndrome decoding setting, (ii) a decoding algorithm is optimized directly over a finite field metric, (iii) a deep neural network is applied to the faulty syndrome decoding task.

Applied to a variety of code lengths, noise and measurement errors, our method outperforms the state-of-the-art method. This performance gain holds even when employing shallow architectures, providing a sizable speedup over the existing neural decoders, which are known to be computationally inefficient (Edmonds, 1965; Dennis et al., 2002).

2. Related Work

Maximum Likelihood quantum decoding is an NP-hard problem (Kuo & Lu, 2020) and several approximation methods have been developed as practical alternatives, trading off the accuracy for greater complexity. The Minimum-Weight Perfect Matching (MWPM) algorithm runs in polynomial time and is known to achieve nearly the optimal threshold for independent noise models (Bose & Dowling, 1969; Micali & Vazirani, 1980). It is formulated as a problem of pairing excitation and can be solved using Blossom's algorithm (Kolmogorov, 2009). Approximations of this algorithm have been developed by parallelizing the group processing or removing edges that are unlikely to contribute

to the matching process. However, MWPM implementations and modifications generally induce degradation in accuracy or are too slow even for the current generation of superconducting qubits (Fowler et al., 2012; Fowler, 2013; Meinerz et al., 2022).

Among other approaches, methods based on Monte Carlo Markov Chains (MCMC) (Wootton & Loss, 2012; Hutter et al., 2014) iteratively modify the error estimate, to increase its likelihood with respect to the received syndrome. Renormalization Group methods (Duclos-Cianci & Poulin, 2010; 2013) perform decoding by dividing the lattice into small cells of qubits. Union-Find decoders (Huang et al., 2020; Delfosse & Nickerson, 2021) iteratively turn Pauli errors into losses that are corrected by the Union-Find data structure and are more suited to other types of noise.

Multiple neural networks-based quantum decoders have emerged in the last few years (Varsamopoulos et al., 2017; Torlai & Melko, 2017; Krastanov & Jiang, 2017; Chamberland & Ronagh, 2018; Andreasson et al., 2019; Wagner et al., 2020; Sweke et al., 2020; Varona & Martin-Delgado, 2020; Meinerz et al., 2022). These methods are amendable to parallelization and can offer a high degree of adaptability. Current contributions make use of multi-layer perceptrons (Varsamopoulos et al., 2017; Torlai & Melko, 2017; Krastanov & Jiang, 2017; Wagner et al., 2020) or relatively shallow convolutional neural networks (Andreasson et al., 2019; Sweke et al., 2020), or couple the decoding with classical methods for boosting the decoding accuracy (Meinerz et al., 2022).

In parallel, deep learning methods have been improving steadily for classical ECC, reaching state-of-the-art results for a broad range of codes. Many of these methods rely on augmenting the Belief-propagation algorithm with learnable parameters (Pearl, 1988; Nachmani et al., 2016; Lugosch & Gross, 2017; Nachmani & Wolf, 2019; Buchberger et al., 2020), while others make use of more general neural network architectures (Cammerer et al., 2017; Gruber et al., 2017; Kim et al., 2018; Bennatan et al., 2018; Choukroun & Wolf, 2023).

Recently, Choukroun & Wolf (2022) have proposed a transformer-based architecture (Vaswani et al., 2017) that is currently the state of the art in neural decoders for classical codes. We choose to address QECC by expanding the ECCT architecture to account for the challenges arising from the transition from classical to quantum neural decoding. Analogous expansions can be applied to other neural decoders.

3. Background

We provide the necessary background on classical and quantum error correction coding and a description of the state-of-

the-art Error Correction Code Transformer (ECCT) decoder.

3.1. Classical Error Correction Code

A linear code C is defined by a binary generator matrix G of size $k \times n$ and a binary parity check matrix H of size $(n-k) \times n$ defined such that $GH^T = 0$ over the order 2 Galois field $GF(2)$.

The input message $m \in \{0, 1\}^k$ is encoded by G to a codeword $x \in C \subset \{0, 1\}^n$ satisfying $Hx = 0$ and transmitted via a symmetric (potentially binary) channel, e.g., an additive white Gaussian noise (AWGN) channel. Let y denote the channel output represented as $y = x_s + \varepsilon \in \mathcal{S} \subseteq \mathbb{R}^n$, where x_s denotes the modulation of x , e.g. Binary Phase Shift Keying (BPSK), and ε is random noise independent of the transmitted x . The main goal of the decoder $f : \mathcal{S} \rightarrow \{0, 1\}^n$ is to provide an approximation of the codeword $\hat{x} = f(y)$.

An important notion in ECC is the syndrome, which is obtained by multiplying the binary mapping of y with the parity check matrix over $GF(2)$ such that

$$s := s(y) = Hy_b := H(x \oplus \varepsilon_b) = H\varepsilon_b, \quad (1)$$

where \oplus denotes the XOR operator, and y_b and ε_b denote the hard-decision vectors of y and ε , respectively. An illustration of the classical ECC framework is presented in Figure 1(a).

3.2. Quantum Error Correction Code

The fundamental transition to the quantum realm is defined by the shift from the classical bit to the quantum bit (qubit), whose quantum state $|\psi\rangle$ is defined by

$$|\psi\rangle = \alpha|0\rangle + \beta|1\rangle, \quad \text{s.t. } \alpha, \beta \in \mathbb{C}, \quad |\alpha|^2 + |\beta|^2 = 1 \quad (2)$$

A coherent quantum error process E can be decomposed into a sum of operators from the Pauli set $\{I, X, Z, XZ\}$, where the Pauli basis is defined by the identity mapping I , the quantum bit-flip X and the phase-flip Z , such that the single-qubit errors are defined as

$$\begin{aligned} I|\psi\rangle &= |\psi\rangle \\ X|\psi\rangle &= \alpha X|0\rangle + \beta X|1\rangle = \alpha|1\rangle + \beta|0\rangle \\ Z|\psi\rangle &= \alpha Z|0\rangle + \beta Z|1\rangle = \alpha|0\rangle - \beta|1\rangle \\ E|\psi\rangle &= \alpha_I|\psi\rangle + \alpha_X X|\psi\rangle + \alpha_Z Z|\psi\rangle + \alpha_{XZ} XZ|\psi\rangle \end{aligned} \quad (3)$$

with $\alpha_I, \alpha_X, \alpha_Z, \alpha_{XZ} \in \mathbb{C}$ being the expansion coefficients of the noise process.

According to the no-cloning theorem, a quantum state $|\psi\rangle$ cannot be copied redundantly (i.e. $|\psi\rangle \otimes \dots \otimes |\psi\rangle$), where $\underbrace{\otimes \dots \otimes}_n$ denotes the n -fold tensor product. However, quantum information redundancy is possible through

a *logical* state encoding $|\psi\rangle_n$ of a given state $|\psi\rangle$ via quantum entanglement and a unitary operator U such that $|\psi\rangle_n = U(|\psi\rangle \otimes |0\rangle \otimes \dots \otimes |0\rangle)$. An example of such a unitary operator is the GHZ state (Greenberger et al., 1989), which is generated with CNOT gates. In $|\psi\rangle_n$, the logical state is defined within a subspace of the expanded Hilbert space, which determines both the codespace \mathcal{C} and its orthogonal error space \mathcal{F} defined such that $E|\psi\rangle_n \in \mathcal{F}$.

The orthogonality of \mathcal{C} and \mathcal{F} makes it possible to determine the subspace occupied by the logical qubit through projective measurement, without compromising the encoded quantum information. In the context of quantum coding, the set \mathcal{P} of non-destructive measurements of this type are called stabilizer measurements and are performed via additional qubits (ancilla bits). The result of all of the stabilizer measurements on a given state is called the *syndrome*, such that for a given stabilizer generator $P \in \mathcal{P}$ we have $P|\psi\rangle_n = |\psi\rangle_n$, and $PE|\psi\rangle_n = -E|\psi\rangle_n, \forall |\psi\rangle_n \in \mathcal{C}$ given an anti-commuting (i.e. -1 eigenvalue) and thus detectable error E . If the syndrome measurement is faulty, it might be necessary to repeat it to improve confidence in the outcome (Dennis et al., 2002, Section IV.B).

An important class of Pauli operators is the class of logical operators. These operators are not elements of the stabilizer group, but commute with every stabilizer. While stabilizers operators act trivially in the code space, i.e. $P|\psi\rangle_n = |\psi\rangle_n$, logical operators $\ell \in \mathcal{L}$ act non-trivially in it, i.e. $\exists |\phi\rangle_n \in \mathcal{C}$ s.t. $\ell|\psi\rangle_n = |\phi\rangle_n$. Such operators commute with the stabilizers but can also represent undetectable errors (Brun, 2020). Thus, QECC benchmarks generally adopt logical error metrics, which measure the discrepancy between the predicted projected noise $\mathbb{L}\hat{\varepsilon}$ and the real one $\mathbb{L}\varepsilon$, where \mathbb{L} is the discrete logical operators' matrix.

QECC from the ECC perspective: Another way to represent stabilizer codes is to split the stabilizer operators into two independent parity check matrices, defining the block parity check matrix H such that $H = \begin{pmatrix} H_Z & 0 \\ 0 & H_X \end{pmatrix}$, separating phase-flip checks H_Z and bit-flip checks H_X . The syndrome s is then computed as $s = H\varepsilon$, H being the check-matrix defined according to the code stabilizers in \mathcal{P} , and ε the binary noise. The main goal of the quantum decoder $f : \{0, 1\}^{|\mathcal{P}|} \rightarrow \{0, 1\}^{|\mathcal{L}|}$ is to provide a noise approximation given only the syndrome.

Therefore, the quantum setting can be reduced to its classical counterpart as follows. The k logical qubits are similar to the classical k information bits, and the n physical qubits are similar to the classical codeword. The syndrome of the quantum state can be computed or simulated similarly to the classical way, by defining the binary parity check matrix built upon the code quantum stabilizers. The main differences from classical ECC are: (i) no access to the

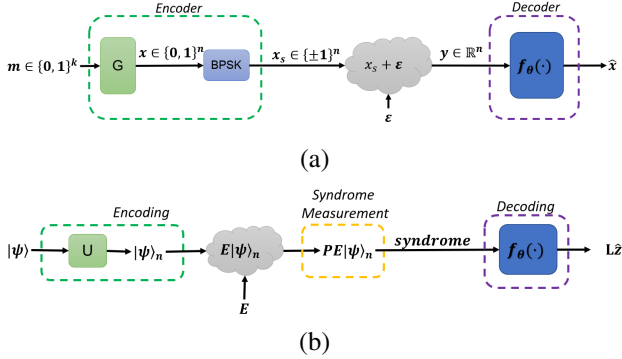


Figure 1. Illustration of the (a) classical and (b) quantum ECC system. Our work focuses on the design and training of the parameterized quantum decoder.

current state is possible, while arbitrary measurement of y is standard in the classical world; (ii) we are interested in the logical qubits, predicting the code up to the logical operators mapping \mathbb{L} ; and finally, (iii) repetitive sampling of the syndrome due to the syndrome measurement error. These differences are at the core of our contributions.

An illustration of the quantum coding and decoding framework is presented in Figure 1(b). The goal of our method is to learn a decoder that is parameterized by a vector of weights θ such that $\hat{\varepsilon} = f_\theta(s)$.

3.3. Error Correction Code Transformer

The state-of-the-art ECCT by Choukroun & Wolf (2022) has been recently proposed for classical error decoding. It consists of a transformer architecture (Vaswani et al., 2017) with several modifications.

Following Bennatan et al. (2018), the model’s input is defined by the concatenation of the codeword-independent magnitude and syndrome, such that $h(y) := [|y|, 1 - 2s(y)] \in \mathbb{R}^{2n-k}$ where $[\cdot, \cdot]$ denotes vector concatenation. Each element is then embedded into a high-dimensional space for more expressivity, such that the initial positional embedding Φ is given by $\Phi = (h(y) \cdot \mathbb{1}_d^T) \odot W$, where $W \in \mathbb{R}^{2n-k \times d}$ is the learnable embedding matrix and \odot is the Hadamard product.

The interaction between the bits is performed naturally via the self-attention modules coupled with a binary mask derived from the parity-check matrix

$$A_H(Q, K, V) = \text{Softmax} \left(\frac{QK^T + g(H)}{\sqrt{d}} \right) V \quad (4)$$

where $g(H)$ is a binary masking function designed according to the parity-check matrix H , and Q, K, V are the classical self-attention projection matrices. Masking enables

the incorporation of sparse and efficient information about the code while avoiding the loop vulnerability of belief propagation-based decoders (Pearl, 1988). Finally, the transformed embedding is projected onto a one-dimensional vector for noise prediction.

4. Method

We present in this Section the elements of the proposed decoding framework, the complete architecture, and the training procedure. From now on, the binary block parity check matrix is denoted by H , the binary noise by ε , the syndrome by $s = H\varepsilon$, and the logical operators’ binary matrix by \mathbb{L} .

4.1. Overcoming Measurement Collapse by Prediction

While syndrome decoding is a well-known procedure in ECC, most popular decoders, and especially neural decoders, assume the availability of arbitrary measurements of the channel’s output. In the QECC setting, only the syndrome is available, since classical measurements are not allowed due to the wave function collapse phenomenon.

We thus propose to extend ECCT, by replacing the magnitude of the channel output y with an initial estimate of the noise. In other words, we replace the channel’s output magnitude measurement $h(y) = [|y|, 1 - 2s]$ by $h_q(s) = [g_\omega(s), s]$.

Denoting the ECCT decoder by f_θ we have

$$\hat{\varepsilon} = f_\theta(h_q(s)) = f_\theta([g_\omega(s), s]), \quad (5)$$

where $g_\omega : \{0, 1\}^{n_s} \rightarrow \mathbb{R}^n$ is the initial noise estimator, given by a shallow neural network parameterized by ω . This way, the ECCT can process the estimated input and perform decoding by analyzing the input-syndrome interactions via the masking. As a non-linear transformation of the syndrome, $g_\omega(s)$ is also independent of the quantum state/codeword and thus robust to overfitting. The estimator $g_\omega(s)$ is trained via the following objective

$$\mathcal{L}_g = \text{BCE}(g_\omega(s), \varepsilon), \quad (6)$$

where BCE is the binary cross entropy loss. This shift from magnitude to initial error estimation is crucial for overcoming quantum measurement collapse and, as is explored in Section 6.2, leads to markedly better performance.

4.2. Logical Decoding

Contrary to classical ECC, quantum error correction aims to restore the noise up to a *logical* generator of the code, such that several solutions can be valid. Accordingly, a commonly used metric is the logical error rate (LER), which provides valuable information on the practical decoding

performance (Lidar & Brun, 2013). Given the code’s logical operator in its matrix form $\mathbb{L} \in \{0, 1\}^{k \times n}$, we wish to minimize the following LER objective

$$\mathcal{L}_{\text{LER}} = \text{BCE}(\mathbb{L}f_{\theta}(s), \mathbb{L}\varepsilon). \quad (7)$$

where the multiplications are performed over $GF(2)$ and are thus highly non-differentiable.

We propose to optimize the objective using a differentiable equivalence mapping of the XOR (i.e., sum over $GF(2)$) operation as follows. Defining the bipolar mapping $\phi : \{0, 1\} \rightarrow \{\pm 1\}$ over $GF(2)$ as $\phi(u) = 1 - 2u, u \in \{0, 1\}$, we obtain the following property $\phi(u \oplus v) = \phi(u)\phi(v), \forall u, v \in \{0, 1\}$. Thus, with \mathbb{L}_i the i -th row of \mathbb{L} and x a binary vector, we have $\forall i \in \{1 \dots k\}$

$$(\Lambda(\mathbb{L}, x))_i := \mathbb{L}_i \oplus x = \phi^{-1} \left(\prod_j \phi((\mathbb{L})_{ij} \cdot x_j) \right). \quad (8)$$

Thus, as a composition of differentiable functions $\Lambda(\mathbb{L}, x)$ is differentiable and we can redefine our training objective as follows

$$\mathcal{L}_{\text{LER}} = \text{BCE} \left(\Lambda(\mathbb{L}, \text{bin}(f_{\theta}(s))), \mathbb{L}\varepsilon \right), \quad (9)$$

where bin denotes the binarization of the soft prediction of the trained model. While many existing works make use of the straight-through estimator (STE) (Bengio et al., 2013) for the binary quantization of the activations, we opt for its differentiable approximation with the sigmoid function (i.e., $\text{bin}(x) = \sigma(x) = (1 + e^{-x})^{-1}$). As shown in our ablation analysis (Sec. 6.2), the performance of the STE is slightly inferior to the sigmoid approach.

In addition to directly minimizing the LER metric, we are interested in noise prediction solutions that are close to the real system noise. We, therefore, suggest regularizing the objective with the classical and popular Bit Error Rate (BER) objective defined as

$$\mathcal{L}_{\text{BER}} = \text{BCE}(f_{\theta}(s), \varepsilon). \quad (10)$$

We further discuss the importance of this regularization in Section 6.2.

Combining the loss terms, the overall objective is given by

$$\mathcal{L} = \lambda_{\text{BER}} \mathcal{L}_{\text{BER}} + \lambda_{\text{LER}} \mathcal{L}_{\text{LER}} + \lambda_g \mathcal{L}_g \quad (11)$$

where $\lambda_{\text{BER}, \text{LER}, g}$ denote the weights of each objective.

4.3. Noisy Syndrome Measurements

In the presence of measurement errors, each syndrome measurement is repeated T times. This gives the decoder input

an additional time dimension. Formally, given binary system noises $\{\varepsilon_t\}_{t=1}^T$ and binary measurement noises $\{\tilde{\varepsilon}_t\}_{t=1}^T$, we have the syndrome s_t at a given time $t \in \mathbb{N}_+$ defined as

$$s_t = (H(x \oplus \varepsilon_1 \oplus \dots \oplus \varepsilon_t)) \oplus \tilde{\varepsilon}_t \quad (12)$$

In order to remain invariant to the number of measurements, we propose to first analyze each measurement separately and then perform global decoding by applying a symmetric pooling function, e.g. an average, in the middle of the neural decoder.

Given a neural network decoder with N layers and the hidden activation tensor $\varphi \in \mathbb{R}^{T \times h \times n \times d_l}$ at layer $l = \lfloor N/2 \rfloor$, the new pooled embedding is given by summation along the first dimension $\tilde{\varphi} = \frac{1}{T} \sum_{t=1}^T \varphi_t$.

The loss \mathcal{L}_g is thus defined as the distance between the pooled embedding and the noise

$$\mathcal{L}_g = \text{BCE} \left(\sum_t g_{\omega}(s_t) / T, \varepsilon \right) \quad (13)$$

Since we are extending the ECCT architecture to its quantum counterpart (QECCCT), the hidden activation tensor is now of shape $\varphi \in \mathbb{R}^{T \times h \times n \times d_l}$ with h the number of self-attention heads, and pooling is performed at the $\lfloor N/2 \rfloor$ Transformer block.

4.4. Architecture and Training

The initial encoding is defined as a d dimensional one-hot encoding of the $n + n_s$ input elements where n is the number of physical qubits and n_s the length of the syndrome. The network g_{ω} is defined as a shallow network with two fully connected layers of hidden dimensions equal to $5n_s$ and with a GELU non-linearity. The decoder is defined as a concatenation of N decoding layers composed of self-attention and feed-forward layers interleaved with normalization layers. In case of faulty syndrome measurements, the $\lfloor N/2 \rfloor$ th layer performs average pooling over the time dimension.

The output is obtained via two fully connected layers. The first layer reduces the element-wise embedding to a one-dimensional $n + n_s$ vector and the second to an n dimensional vector representing the soft decoded noise, trained over the objective given Eq. 11. An illustration of the proposed QECCCT is given in Figure 2. The complexity of the network is linear with the code length n and quadratic with the embedding dimension d and is defined by $\mathcal{O}(Nd^2n)$ for sparse (e.g. topological) codes. The acceleration of the proposed method (e.g. pruning, quantization, distillation) (Wang et al., 2020; Lin et al., 2021) is left for future work.

The Adam optimizer (Kingma & Ba, 2014) is used with 128 samples per minibatch, for 200 to 400 epochs depending on the code length, with 5000 minibatches per epoch.

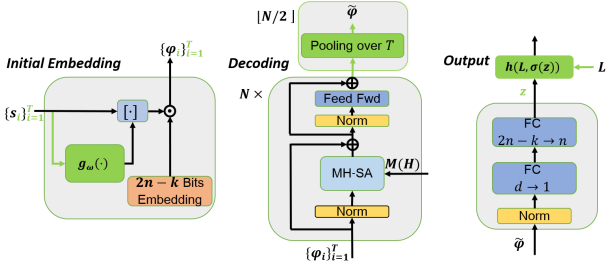


Figure 2. Illustration of the proposed Quantum Error Correction Code Transformer architecture (QECCCT). The main modifications are indicated in green. The pooling layer is performed only after the middle self-attention block of the model and $M(H)$ denotes the adapted mask from the parity-check matrix.

The noise is sampled randomly per batch in the physical error rate testing range. The default weight parameters are $\lambda_g = 0.5$, $\lambda_{\text{LER}} = 1$, $\lambda_{\text{BER}} = 0.5$. Other configurations and longer training can be beneficial but were not tested due to a lack of computational resources. The default architecture is defined by $N = 6$, $d = 128$.

We initialized the learning rate to $5 \cdot 10^{-4}$ coupled with a cosine decay scheduler down to $5 \cdot 10^{-7}$ at the end of training. No warmup (Xiong et al., 2020) was employed. Training and experiments were performed on a 12GB Titan V GPU. The training time is in the range of 153 to 345 seconds per epoch for the 8 to 128 code lengths, respectively with the default architecture. Test time is in the range of 0.1 to 0.6 milliseconds per sample. The number of testing samples is set to 10^5 . No optimization of the sparse self-attention mechanism was employed.

5. Application to Topological Codes

While our framework is universal in terms of the code, we focus on the popular surface codes and, more specifically, on Toric codes (Kitaev, 1997a;c; 2003), which are their variant with periodic boundary conditions. These codes are among the most attractive candidates for quantum computing experimental realization, as they can be implemented on a two-dimensional grid of qubits with local check operators (Bravyi et al., 2018). The physical qubits are placed on the edges of a two-dimensional lattice of length L , such that the stabilizers are defined with respect to the code lattice architecture that defines the codespace, where $n = 2L^2$.

The stabilizers are defined in two groups: vertex operators are defined on each *vertex* as the product of X operators on the adjacent qubits and *plaquette* operators are defined on each face as the product of Z operators on the bordering qubits. Therefore, there exist a total of $2L^2$ stabilizers, L^2 for each stabilizer group. Assuming that a qubit is associated

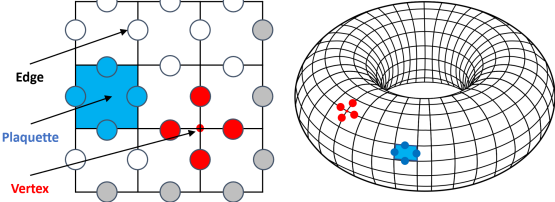


Figure 3. The lattice representation of the $(k=3)$ Toric code and its embedding into a three-dimensional torus. Gray edges represent periodic boundaries.

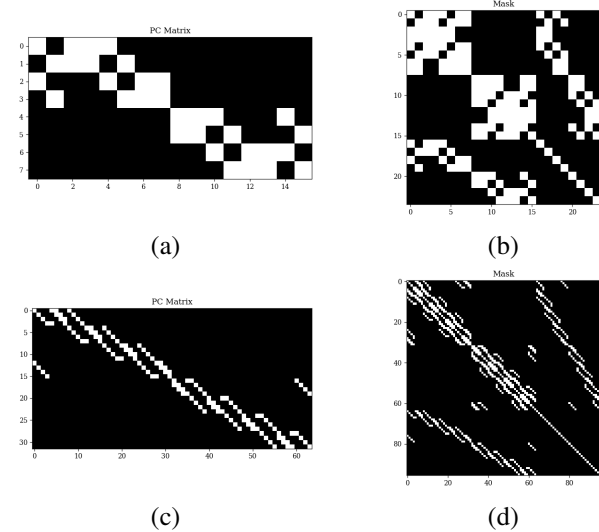


Figure 4. (a) The parity-check matrix and (b) the induced masking for the 2-Toric code. (c,d) the corresponding matrix and mask for the 4-Toric code. The parity check matrix comprises two block matrices for the X and Z stabilizers. We can observe the high locality and sparsity of the Toric code.

with every edge of the lattice, for a given vertex v we have the vertex operator defined as $X_v = \prod_{i \in v} X_i$, and for a given plaquette p , the plaquette operator defined as $Z_p = \prod_{i \in p} Z_i$. An illustration is given in Figure 3.

The mask is defined such that the self-attention mechanism only takes into consideration bits related to each other in terms of the stabilizers (i.e., the parity-check matrix). The parity-check matrices and their corresponding masks for several Toric codes are provided in Figure 4, where one can observe the high locality induced by the code architecture.

6. Experiments

We evaluate our method on various toric codes, considering the two common noise models: independent and depolarization. In independent (uncorrelated) noise, X and Z errors occur independently and with equal probabilities; therefore, decoding can be performed on the

X or Z stabilizers separately. Depolarization noise assigns equal probability $p/3$ to all three Pauli operators $\mathbb{P}(X) = \mathbb{P}(Z) = \mathbb{P}(Y) = p/3, \mathbb{P}(I) = 1 - p$, where Y is the Pauli operator defined as $Y = iXZ$.

In the experiments where measurement errors are incorporated, each syndrome measurement is repeated $T = n$ times and the probability of the measurement error is the same as the probability of the syndrome error, i.e., the distributions of ε and $\tilde{\varepsilon}$ in Eq. 12 are the same.

The implementation of the Toric codes is taken from (Krasstanov & Jiang, 2017). As a baseline, we consider the Minimum-Weight Perfect Matching (MWPM) algorithm with the complexity of $\mathcal{O}(n^3)$, also known as the Edmond or Blossom algorithm, which is the most popular decoder for topological codes. Its implementation is taken from (Higgott & Gidney, 2022; Higgott, 2022). In the experiments, we employ code lengths similar to those for which the existing neural decoders were tested (Varsamopoulos et al., 2017; Torlai & Melko, 2017; Krasstanov & Jiang, 2017; Chamberland & Ronagh, 2018; Andreasson et al., 2019; Wagner et al., 2020). It is worth noting that none of these previous methods outperform MWPM. The physical error ranges are taken around the thresholds of the different settings, as reported in (Dennis et al., 2002; Wang et al., 2003; Krasstanov & Jiang, 2017). On the tested codes and settings, the Union-find decoder (Park & Meinerz, 2022) was not better than the MWPM algorithm.

As metrics, we present both the bit error rates (BER) and the logical error rate (LER), see Sec. 4.2. The LER metric here is a word-level error metric, meaning there is an error if at least one qubit is different from the ground truth. Unless stated otherwise, we use the $N = 6, d = 128$ architecture.

Larger architectures that can be used for larger codes would be possible and beneficial in terms of accuracy, given the necessary computational resources. For example, GPT-3 (Brown et al., 2020) successfully operates on 2K inputs with a similar Transformer model but with $N = 96, d = 12K$.

6.1. Results

Figure 5 depicts the performance of the proposed method and the MWPM algorithm for different Toric code lengths under the *independent* noise model and *without* noisy measurements. Figure 6 presents a similar comparison *with* noisy measurements with $T = L$ and uniformly distributed syndrome error. Figure 7 and 8 compare our method with MWPM for the *depolarized* noise model, with and without noisy measurements, respectively.

As can be seen, the proposed QECCT outperforms the state-of-the-art MWPM algorithm by a large margin. However, as mentioned above, these experiments do not fully expose the full potential of the method: our runs are heavily restricted

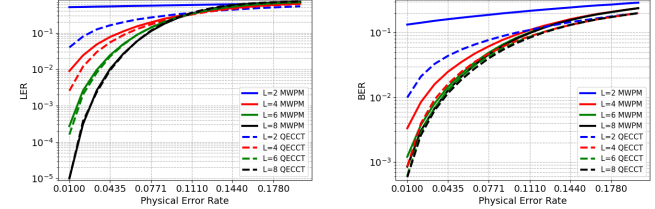


Figure 5. LER and BER performance for various physical error rates and lattice length on the Toric code with *independent* noise and *without* faulty syndrome measurements.

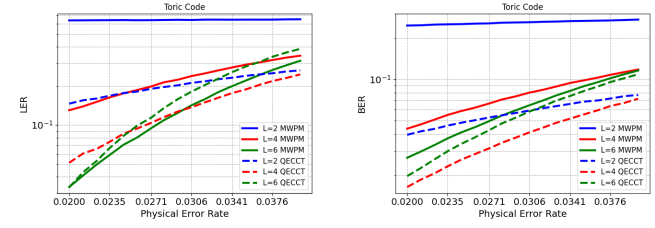


Figure 6. LER and BER performance for various physical error rates and lattice length on the Toric code with *independent* noise and *with* faulty syndrome measurements.

by computational resources, and as the code length increases it would be beneficial to use models with larger capacity and to employ longer training sessions.

6.2. Exploratory experiments

Impact of the noise estimator g_ω Figure 9(a) explores the impact of g_ω on performance. Since in order to use the QECCT the initial scaling estimate needs to be defined, we compare our approach to constant scaling with ones, meaning $g_\omega := \mathbb{1}_n$. We further explore two architectures for g_ω : one with a single hidden layer and one with three hidden layers. Evidently, the initial noise estimator is critical for performance. However, the network architecture is less impactful. Given more resources, one can check the impact of additional architectures.

Impact of the various objectives Figure 10(a) depicts the impact of the different loss terms in Eq. 11. First, we can observe that training solely with the \mathcal{L}_{LER} objective converges rapidly to a bad local minimum. This is illustrated in Figure 10(b) where we display the gradient norm average over the network layers.

We hypothesize that this issue may be due to the fact that the dimension of the LER objective is rather small and the gradients can collapse in the product of the code elements in Eq 8, since $\sigma(x)^n \xrightarrow{n \rightarrow \infty} 0$.

Evidently, training with \mathcal{L}_{BER} only produces far worse results than combining it with the \mathcal{L}_{LER} objective. For

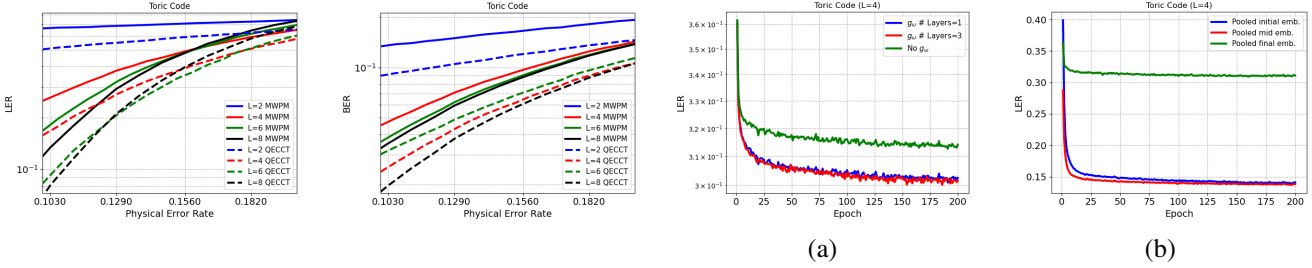


Figure 7. LER and BER performance for various error physical rates and lattice length on the Toric code with *depolarization* noise and *without* faulty syndrome measurements.

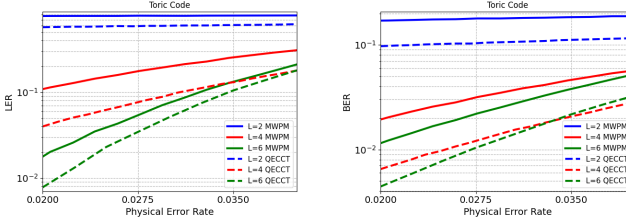


Figure 8. LER and BER performance for various error physical rates and lattice length on the Toric code with *depolarization* noise and *with* faulty syndrome measurements.

high SNR, a model trained with \mathcal{L}_{BER} objective yields a 27 times higher LER than the model trained with combined objectives. Moreover, optimizing with the noise estimator objective \mathcal{L}_g results, for high SNR, in a 46% improvement over not employing regularization.

Impact of Pooling Figure 9(b) depicts the impact of different pooling (averaging) scenarios. Pooling is performed either after the initial embedding, in the middle of the network, or over the final embedding. Evidently, performing pooling in the middle layer allows better decoding. Pooling the final embedding (similarly to voting) is not effective.

Impact of the Mask and the Architecture Finally, we present the impact of masking in Figure 11(a) and the impact of the model’s capacity and the performance of the STE as *bin* function from Eq 9 in Figure 11(b). We can observe that while less important than with classical codes (Choukroun & Wolf, 2022), the mask still has a substantial impact on performance. Also, we note that increasing the capacity of the network enables better representation and decoding.

7. Conclusion

We present a novel Transformer-based framework for decoding quantum codes. The proposed approach enables effective representation and training under the QECC constraints. The framework helps overcome the measurement collapse phenomenon, such that a Transformer architecture can be employed, combined with efficient and size-invariant

Figure 9. Impact of the g_ω on LER performance during training with an $N = 6, d = 128$ architecture (a). "No g_ω " refers to constant mapping, i.e., $g_\omega = \mathbb{1}_n$. Impact of pooling (averaging) performed at different levels of the network for a $N = 6, d = 128$ model (b). The average final testing LER of mid-level pooling is 5% lower than the initial embedding pooling.

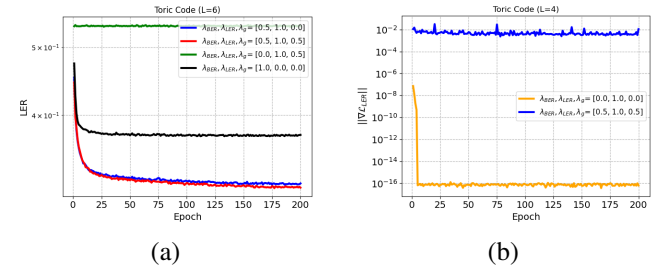


Figure 10. Impact of the different loss terms on performance (a). Impact of regularization on the training dynamics (b) with a $N = 6, d = 128$ model.

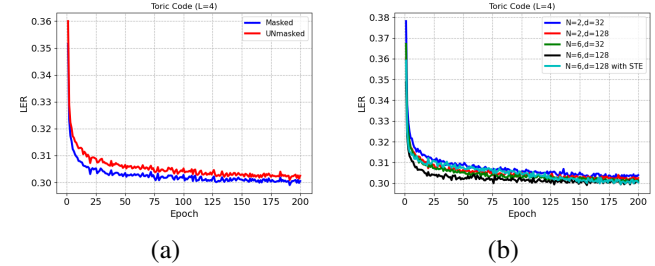


Figure 11. (a) Impact of masking on accuracy with an $N = 2, d = 128$ model. (b) Impact of the model size on accuracy with an $N = 6, d = 128$ model. We also provide the performance of the STE as the *bin* function.

pooling for faulty measurement scenarios. A major contribution is the differentiable training of highly non-differentiable functions present in every error correction setting. The proposed framework is the first neural decoder to outperform the state-of-the-art classical methods. Since the lack of effective and efficient error correction is a well-known limiting factor for the development of quantum computers, our contribution can play a role in using machine learning tools for overcoming the current technological limitations of many qubit systems.

References

Aharonov, D. and Ben-Or, M. Fault-tolerant quantum computation with constant error. In *Proceedings of the twenty-ninth annual ACM symposium on Theory of computing*, pp. 176–188, 1997.

Andreasson, P., Johansson, J., Liljestrand, S., and Granath, M. Quantum error correction for the toric code using deep reinforcement learning. *Quantum*, 3:183, 2019.

Ballance, C., Harty, T., Linke, N., Sepiol, M., and Lucas, D. High-fidelity quantum logic gates using trapped-ion hyperfine qubits. *Physical review letters*, 117(6):060504, 2016.

Bengio, Y., Léonard, N., and Courville, A. Estimating or propagating gradients through stochastic neurons for conditional computation. *arXiv preprint arXiv:1308.3432*, 2013.

Bennatan, A., Choukroun, Y., and Kisilev, P. Deep learning for decoding of linear codes-a syndrome-based approach. In *2018 IEEE International Symposium on Information Theory (ISIT)*, pp. 1595–1599. IEEE, 2018.

Bose, R. C. and Dowling, T. *Combinatorial mathematics and its applications: proceedings of the conference held at the University of North Carolina at Chapel Hill, April 10-14, 1967*. Number 4. University of North Carolina Press, 1969.

Bravyi, S., Englbrecht, M., König, R., and PEARD, N. Correcting coherent errors with surface codes. *npj Quantum Information*, 4(1):1–6, 2018.

Bravyi, S. B. and Kitaev, A. Y. Quantum codes on a lattice with boundary. *arXiv preprint quant-ph/9811052*, 1998.

Brown, T., Mann, B., Ryder, N., Subbiah, M., Kaplan, J. D., Dhariwal, P., Neelakantan, A., Shyam, P., Sastry, G., Askell, A., et al. Language models are few-shot learners. *Advances in neural information processing systems*, 33: 1877–1901, 2020.

Brun, T. A. Quantum error correction, 02 2020. URL <https://oxfordre.com/physics/view/10.1093/acrefore/9780190871994.001.0001/acrefore-9780190871994-e-35>.

Buchberger, A., Häger, C., Pfister, H. D., Schmalen, L., et al. Learned decimation for neural belief propagation decoders. *arXiv preprint arXiv:2011.02161*, 2020.

Calderbank, A. R. and Shor, P. W. Good quantum error-correcting codes exist. *Physical Review A*, 54(2):1098, 1996.

Cammerer, S., Gruber, T., Hoydis, J., and ten Brink, S. Scaling deep learning-based decoding of polar codes via partitioning. In *GLOBECOM 2017-2017 IEEE Global Communications Conference*, pp. 1–6. IEEE, 2017.

Chamberland, C. and Ronagh, P. Deep neural decoders for near term fault-tolerant experiments. *Quantum Science and Technology*, 3(4):044002, 2018.

Choukroun, Y. and Wolf, L. Error correction code transformer. *Advances in Neural Information Processing Systems (NeurIPS)*, 2022.

Choukroun, Y. and Wolf, L. Denoising diffusion error correction codes. *International Conference on Learning Representations (ICLR)*, 2023.

Cory, D. G., Price, M., Maas, W., Knill, E., Laflamme, R., Zurek, W. H., Havel, T. F., and Somaroo, S. S. Experimental quantum error correction. *Physical Review Letters*, 81(10):2152, 1998.

Delfosse, N. and Nickerson, N. H. Almost-linear time decoding algorithm for topological codes. *Quantum*, 5: 595, 2021.

Dennis, E., Kitaev, A., Landahl, A., and Preskill, J. Topological quantum memory. *Journal of Mathematical Physics*, 43(9):4452–4505, 2002.

Duclos-Cianci, G. and Poulin, D. Fast decoders for topological quantum codes. *Physical review letters*, 104(5): 050504, 2010.

Duclos-Cianci, G. and Poulin, D. Fault-tolerant renormalization group decoder for abelian topological codes. *arXiv preprint arXiv:1304.6100*, 2013.

Edmonds, J. Paths, trees, and flowers. *Canadian Journal of mathematics*, 17:449–467, 1965.

Fowler, A. G. Minimum weight perfect matching of fault-tolerant topological quantum error correction in average $o(1)$ parallel time. *arXiv preprint arXiv:1307.1740*, 2013.

Fowler, A. G., Whiteside, A. C., and Hollenberg, L. C. Towards practical classical processing for the surface code. *Physical review letters*, 108(18):180501, 2012.

Foxen, B., Neill, C., Dunsworth, A., Roushan, P., Chiaro, B., Megrant, A., Kelly, J., Chen, Z., Satzinger, K., Barends, R., et al. Demonstrating a continuous set of two-qubit gates for near-term quantum algorithms. *Physical Review Letters*, 125(12):120504, 2020.

Freedman, M. H. and Meyer, D. A. Projective plane and planar quantum codes. *Foundations of Computational Mathematics*, 1(3):325–332, 2001.

Gottesman, D. *Stabilizer codes and quantum error correction*. California Institute of Technology, 1997.

Greenberger, D. M., Horne, M. A., and Zeilinger, A. Going beyond bell's theorem. In *Bell's theorem, quantum theory and conceptions of the universe*, pp. 69–72. Springer, 1989.

Gruber, T., Cammerer, S., Hoydis, J., and ten Brink, S. On deep learning-based channel decoding. In *2017 51st Annual Conference on Information Sciences and Systems (CISS)*, pp. 1–6. IEEE, 2017.

Higgott, O. Pymatching: A python package for decoding quantum codes with minimum-weight perfect matching. *ACM Transactions on Quantum Computing*, 3(3):1–16, 2022.

Higgott, O. and Gidney, C. Pymatching v2. <https://github.com/oscarhiggott/PyMatching>, 2022.

Huang, S., Newman, M., and Brown, K. R. Fault-tolerant weighted union-find decoding on the toric code. *Physical Review A*, 102(1):012419, 2020.

Huang, W., Yang, C., Chan, K., Tanttu, T., Hensen, B., Leon, R., Fogarty, M., Hwang, J., Hudson, F., Itoh, K. M., et al. Fidelity benchmarks for two-qubit gates in silicon. *Nature*, 569(7757):532–536, 2019.

Hutter, A., Wootton, J. R., and Loss, D. Efficient markov chain monte carlo algorithm for the surface code. *Physical Review A*, 89(2):022326, 2014.

Kim, H., Jiang, Y., Rana, R., Kannan, S., Oh, S., and Viswanath, P. Communication algorithms via deep learning. In *Sixth International Conference on Learning Representations (ICLR)*, 2018.

Kingma, D. P. and Ba, J. Adam: A method for stochastic optimization. *arXiv preprint arXiv:1412.6980*, 2014.

Kitaev, A. Y. Quantum computations: algorithms and error correction. *Russian Mathematical Surveys*, 52(6):1191, 1997a.

Kitaev, A. Y. Quantum error correction with imperfect gates. In *Quantum communication, computing, and measurement*, pp. 181–188. Springer, 1997b.

Kitaev, A. Y. Quantum computations: algorithms and error correction. *Russian Mathematical Surveys*, 52(6):1191, 1997c.

Kitaev, A. Y. Fault-tolerant quantum computation by anyons. *Annals of Physics*, 303(1):2–30, 2003.

Kolmogorov, V. Blossom v: a new implementation of a minimum cost perfect matching algorithm. *Mathematical Programming Computation*, 1(1):43–67, 2009.

Krastanov, S. and Jiang, L. Deep neural network probabilistic decoder for stabilizer codes. *Scientific reports*, 7(1):1–7, 2017.

Kuo, K.-Y. and Lu, C.-C. On the hardnesses of several quantum decoding problems. *Quantum Information Processing*, 19(4):1–17, 2020.

Lidar, D. A. and Brun, T. A. *Quantum error correction*. Cambridge university press, 2013.

Lin, T., Wang, Y., Liu, X., and Qiu, X. A survey of transformers. *arXiv preprint arXiv:2106.04554*, 2021.

Lugosch, L. and Gross, W. J. Neural offset min-sum decoding. In *2017 IEEE International Symposium on Information Theory (ISIT)*, pp. 1361–1365. IEEE, 2017.

MacKay, D. J., Mac Kay, D. J., et al. *Information theory, inference and learning algorithms*. Cambridge university press, 2003.

Meinerz, K., Park, C.-Y., and Trebst, S. Scalable neural decoder for topological surface codes. *Physical Review Letters*, 128(8):080505, 2022.

Micali, S. and Vazirani, V. V. An o (v—v—c—e—) algorithm for finding maximum matching in general graphs. In *21st Annual Symposium on Foundations of Computer Science (sfcs 1980)*, pp. 17–27. IEEE, 1980.

Nachmani, E. and Wolf, L. Hyper-graph-network decoders for block codes. In *Advances in Neural Information Processing Systems*, pp. 2326–2336, 2019.

Nachmani, E., Be’ery, Y., and Burshtein, D. Learning to decode linear codes using deep learning. In *2016 54th Annual Allerton Conference on Communication, Control, and Computing (Allerton)*, pp. 341–346. IEEE, 2016.

Neumann, J., Wigner, E. P., and Hofstadter, R. *Mathematical foundations of quantum mechanics*. Princeton university press, 1955.

Nielsen, M. A. and Chuang, I. Quantum computation and quantum information, 2002.

Park, C.-Y. and Meinerz, K. Open-source c++ implementation of the union-find decoder, <https://github.com/chaeyeunpark/UnionFind>. *Physical Review Letters*, 128(8):080505, 2022.

Pearl, J. *Probabilistic reasoning in intelligent systems: networks of plausible inference*. Morgan kaufmann, 1988.

Preskill, J. Reliable quantum computers. *Proceedings of the Royal Society of London. Series A: Mathematical, Physical and Engineering Sciences*, 454(1969):385–410, 1998.

Raimond, J. and Haroche, S. Quantum computing: dream or nightmare. *DARK MATTER IN COSMOLOGY QUANTUM MEASUREMENTS EXPERIMENTAL GRA VITA TION*, pp. 341, 1996.

Schindler, P., Barreiro, J. T., Monz, T., Nebendahl, V., Nigg, D., Chwalla, M., Hennrich, M., and Blatt, R. Experimental repetitive quantum error correction. *Science*, 332(6033):1059–1061, 2011.

Shannon, C. E. A mathematical theory of communication. *The Bell system technical journal*, 27(3):379–423, 1948.

Shor, P. W. Scheme for reducing decoherence in quantum computer memory. *Physical review A*, 52(4):R2493, 1995.

Sweke, R., Kesselring, M. S., van Nieuwenburg, E. P., and Eisert, J. Reinforcement learning decoders for fault-tolerant quantum computation. *Machine Learning: Science and Technology*, 2(2):025005, 2020.

Torlai, G. and Melko, R. G. Neural decoder for topological codes. *Physical review letters*, 119(3):030501, 2017.

Varona, S. and Martin-Delgado, M. A. Determination of the semion code threshold using neural decoders. *Physical Review A*, 102(3):032411, 2020.

Varsamopoulos, S., Criger, B., and Bertels, K. Decoding small surface codes with feedforward neural networks. *Quantum Science and Technology*, 3(1):015004, 2017.

Vaswani, A., Shazeer, N., Parmar, N., Uszkoreit, J., Jones, L., Gomez, A. N., Kaiser, Ł., and Polosukhin, I. Attention is all you need. In *Advances in neural information processing systems*, pp. 5998–6008, 2017.

Wagner, T., Kampermann, H., and Bruß, D. Symmetries for a high-level neural decoder on the toric code. *Physical Review A*, 102(4):042411, 2020.

Wang, C., Harrington, J., and Preskill, J. Confinement-higgs transition in a disordered gauge theory and the accuracy threshold for quantum memory. *Annals of Physics*, 303(1):31–58, 2003.

Wang, S., Li, B. Z., Khabsa, M., Fang, H., and Ma, H. Linformer: Self-attention with linear complexity. *arXiv preprint arXiv:2006.04768*, 2020.

Wootters, W. K. and Zurek, W. H. A single quantum cannot be cloned. *Nature*, 299(5886):802–803, 1982.

Wootton, J. R. and Loss, D. High threshold error correction for the surface code. *Physical review letters*, 109(16):160503, 2012.

Xiong, R. et al. On layer normalization in the transformer architecture. *arXiv:2002.04745*, 2020.